Available online at www.sciencedirect.com
SCIENCE DIRECT®
PERGAMON
International Journal of Heat and Mass Transfer 46 (2003) 1503–1517
International Journal of HEAT and MASS TRANSFER
www.elsevier.com/locate/ijhmt

Numerical simulations of hydrodynamics and convective heat transfer in a turbulent tube mist flow

V.I. Terekhov *, M.A. Pakhomov

Kutateladze Institute of Thermophysics SB RAS, 1, Acad. Lavrent'ev Avenue, Novosibirsk 630090, Russia

Received 28 October 2002

Abstract

A computation model is developed, and flow dynamics and heat and mass transfer in a turbulent two-phase gas–drop ducted flow are numerically studied. To calculate the turbulent characteristics of the gas phase, the two-equation Nagano–Tagawa E–ε model was used, modified so that to account for presence of liquid drops in the flow. The impact of various parameters on heat transfer intensification is analyzed. An increase in the gas concentration in the vapor–gas mixture enhances the rate of heat transfer over the initial length of the duct and reduces the length of the evaporation zone. The computed flow dynamics and heat- and mass transfer data are compared with previously reported experimental and numerical results, and a fairly good agreement between the compared data is obtained.

1. Introduction

Multiphase flows and, in particular, two-phase flows are often met in nature and widely used in current technology. Motion of liquid drops in clouds and mists, and interaction between atmosphere and ocean provide examples of natural two-phase flows. Among most important technical applications of two-phase flows are atomization of liquid propellant particles and protection of working surfaces in engines, and also their use in power-equipment components, in chemical apparatus, and in air-conditioning systems. The involvement of a liquid phase and its evaporation in the boundary-layer flow necessitates taking into account the heat and mass transfer between phases. A detailed study of the mechanism underlying the transfer between phases is of especial interest for the supercritical region of the flows in steam-generating devices, when the near-wall film disintegrates and the dispersion-annular mode of the flow gives way to the purely dispersion flow mode [1].

Of primary importance here, especially for technical applications of the flows of interest, is the fact that rather pronounced intensification effects can be achieved with relatively low mass concentrations of the liquid. As a rule, the mass concentration of the liquid phase is no higher than several percents, whereas the heat transfer intensity may be increased by a factor of 3–8. Indicative of such a pronounced intensification are experimental and numerical heat transfer data obtained for two-phase flows around cylinders [1,2], wedge-shaped bodies [3], and plates [4,5], and for two-phase impact jets [6]. Similar effects were also observed when studying ducted flows of vapor–drop [7,8] and gas–drop [9–13] mixtures, both laminar and turbulent.

The heat transfer intensification mechanism operating in the case of the heat carriers of interest consists in making use of the latent evaporation heat being released as the generated vapor undergoes condensation. However, the liquid–drop evaporation process is sensitive to many thermal and gas dynamic parameters [8], which makes theoretical treatment of the combined heat and mass transfer in vapor–gas–drop flows around plates or in ducted vapor–gas–drop flows a difficult problem. That is why a great number of simplifying assumptions were adopted in available numerical studies, which does not allow a rigorous heat- and mass transfer theory to be

* Corresponding author. Tel.: +7-3832-341736/328969; fax: +7-3832-343480.
E-mail address: terekhov@itp.nsc.ru (V.I. Terekhov).

0017-9310/03/$ - see front matter
PII: S0017-9310(02)00472-6

Nomenclature

A	drop area cross-section (m^2), $\pi d^2/4$
b_{1D}	diffusional injection parameter for the vapor released by an evaporation, $(K_V^* - K_V)/(1 - K_V^*)$
C_D	coefficient of resistance
$C_f/2$	skin friction coefficient, $\frac{(\mu+\mu_T)(\partial U/\partial r)_W}{\rho U_{0,m}^2}$
C_p, C_{pA}, C_{pL}, C_{pV}	heat capacities of mixture, air, liquid, and vapor (J/kg K)
D	vapor diffusivity in air (m^2/s)
d	drop diameter (m)
d_P	particle diameter (m)
E	turbulent kinetic energy (m^2/s^2)
F	drop area (m^2), πd^2
g	gravitational acceleration (m/s^2)
G	mass flow rate (kg/s)
G_E	mass flow rate from evaporating drop (kg/s)
J	mass flux of vapor from the surface of evaporating drop (kg/(ms))
k_L	drop deposition velocity (m/s)
K_A, K_V	mass concentration of air and vapor in binary vapor–air mixture
K_V^*	mass concentration of vapor at the drop surface an evaporating corresponding to saturation parameters at the drop temperature T_L
l	mixing length (m)
L	heat of vaporization (J/kg)
m	drop mass (kg), $\rho_L \pi d^3/6$
M_A, M_V, M_L	air, vapor, and liquid mass concentration in the triple air–vapor–drops mixture
n	numerical density of drops (m^{-3}), $\frac{\rho M_{L1}}{\rho_L \pi d_1^3/6}$
Nu	Nusselt number, $\alpha 2R/\lambda$
Nu_L	drop Nusselt number, $\alpha d/\lambda$
Nu_P	Nusselt number non-evaporating particle, $\alpha_P d_P/\lambda$
P	pressure (N/m^2)
Pr	Prandtl number, $C_p\mu/\lambda$
q_E	heat spent on evaporation of liquid drops in the flow (W/m^2)
q_F	heat spent on heating the vapor–gas flow (W/m^2)
q_W	heat flux density supplied to the wall (W/m^2)
q_{WF}	heat flux density supplied to the gas–vapor–drop flow (W/m^2)
q_{WL}	heat flux density due to the conductive heat transfer upon immediate drop/wall contacts (W/m^2)
$\Re$	absolute gas constant (J/(mol K))
R	tube radius (m)
R_+	dimensionless tube radius, RU_*/ν
Re_L	drop Reynolds number, $\rho d \times \sqrt{(U-U_L)^2+(V-V_L)^2}/\mu$
Re_P	Reynolds number of non-evaporating particle, $\rho d_P \sqrt{(U-U_P)^2+(V-V_P)^2}/\mu$
Re_T	turbulence Reynolds number, $E^2/\epsilon\nu$
U, V	velocity component in axial and radial directions (m/s)
U_m	vapor–air mixture mean velocity (m/s)
ΔU	relative velocity of the two phases (m/s), $U - U_L$
U_*	wall friction velocity (m/s)
Sc	Schmidt number, ν/D
Sh	Sherwood number, $\beta d/D$
St_D	diffusional Stanton number, $-\rho_V D\frac{\partial K_V^*}{\partial r}/\rho U(K_V^* - K_V)$
T, T_L	mixture and drop temperatures (K)
W	correction factor for the Stokes law, $(1 + Re_L^{2/3}/6)$
$\langle u^2\rangle$, $\langle v^2\rangle$	root-mean-square velocity fluctuations in axial and radial directions (m^2/s^2)
We	Weber number, $\rho\Delta U^2 d/\sigma$
y	coordinate normal to the wall (m)
y_+	dimensionless distance from the duct wall, written in dynamic variables, $(R-r)U_*/\nu$

Greek symbols

α	heat transfer coefficient (W/(m^2 K))
β	mass transfer coefficient (m/s)
δ	boundary layer thickness (m)
ε	dissipation rate of turbulent kinetic energy (m^2/s^3)
λ	thermal conductivity (W/(m K))
μ	dynamic viscosity ((N s)/m^2)
μ_T	eddy viscosity ((N s)/m^2)
ν	kinematic viscosity (m^2/s)
Θ	relative temperature profile
Ω^ε	time microscale (s), $(15\nu/\epsilon)^{1/2}$
Ω^E	Eulerian time macroscale (s)
Ω^L	Lagrangian time macroscale (s)
ρ, ρ_L, ρ_V	mixture, liquid, vapor densities (kg/m^3)
σ	surface tension (N/m)
τ	particle relaxation time (s), $\rho_L d^2/(18\mu W)$

Subscripts

0	parameter at the duct axis
1	parameter under inlet conditions
A	air
C	critical value of a parameter
D	diffusional parameter
i	current calculation cross-section along the axial direction

$i-1$	previous calculation cross-section along the axial direction	V	vapor
L	drop	W	parameter under condition at the wall
m	mean-mass parameter	$*$	parameter under saturation condition
P	non-evaporating particle	$+$	denotes the dimensionless variables in dynamic universal units
T	turbulent parameter		

developed even for a physically more simple case of a laminar flow. This point was discussed in more detail in [7–13].

With a non-condensable gas present in the mixture, there arises an additional mechanism responsible for the vapor diffusion from the surface of liquid drops into the vapor–gas mixture. The presence of a second component in the gas phase, for instance, air mixed with water vapor, substantially complicates the problem since in this case there arises a need in joint solution of energy and diffusion equations for the vapor–gas phase.

Many works (see, for instance, [1–13]) have been devoted to the theoretical and experimental study of heat transfer in two-phase laminar and turbulent flows and the hydrodynamics of such flows. Among many types of flows, most thoroughly studied are vapor–drop flows, both laminar and turbulent [7,8]. Simultaneously, of primary significance for practical applications is gaining data for ducted turbulent gas–drop flows, although reported studies in this research area are few in number [9–13].

Ganic et al. [9,13] performed a series of experimental and numerical heat transfer studies of ducted gas–drop flows. A good agreement between the measured and theoretically predicted wall temperatures shows that the rate of heat transfer between the wall and the drops depends predominantly on the steady-state wall temperature. The local heat transfer coefficient decreases with increasing wall temperature and increasing wall heat-flux density, and increases with increasing flow velocity and concentration of liquid drops.

Terekhov et al. [11] considered heat and mass transfer in a turbulent, fully developed two-component vapor–gas–drop flow. The turbulent gas phase structure was modeled using the algebraic model of turbulence previously proposed by Deissler [14]. The liquid drops were assumed to exert no substantial influence on the velocity and turbulent-viscosity profiles of the gas flow. In this study, a single-velocity model was used, in which velocities of both phases were assumed identical. This approach has allowed the authors to simplify the problem since in this case it was not necessary to solve the equations of flow for the phase-carrier and the equations of motion for the particles together with the energy and diffusion equations for the vapor–gas mixture.

Many numerical heat transfer studies of gas–vapor–drop flows [9,10] were based on a number of simplifying assumptions that still require a detailed substantiation. For instance, the integral approach [9] and the asymptotic theory of turbulent boundary layer [10], as applied to the description of heat- and mass transfer processes in two-phase flows, do not allow one to take an adequate account of all specific features of the processes in full measure.

Models based on using systems of differential boundary layer equations for two-phase, two-component mixture lack most of such drawbacks. As it was shown in [11,12], such models accurately predict various characteristics of heat- and mass transfer processes in two-component gas–vapor–drop flows.

The problem statement in the present study was much the same as in [11]; however, to close the governing equations, a two-equation E–ϵ model of turbulence [15] was used. Two-equation models of turbulence modified so as to cover the case of flows with a dispersed phase were successfully used to model non-isothermal flows with solid particles [16–18]. At the same time, their applications to the systems with liquid drops are very rare [19].

In the present work, we take into account the influence of many factors on heat transfer, such as precipitation of liquid drops and their evaporation in the duct volume and at the duct surface. Results of testing the model and comparing them with earlier experimental and numerical data are reported.

2. Physical model

We consider a ducted turbulent gas–vapor–drop flow and the heat transfer in it with allowance for the evaporation of liquid drops, interaction between the phases, precipitation of liquid particles onto the duct wall, their heat transfer with the wall, and vapor diffusion into the vapor–gas mixture.

We assume that the annular liquid film on the wall surface has dried already, so that the wall temperature T_W is always higher than the Leidenfrost temperature of the drops [1]. Due to its low intensity, the radiative heat transfer is ignored [7–12]. Next, we assume that all drops undergo instantaneous evaporation as they arrive at the wall, and the duct surface always remains dry; accordingly, there is no liquid film on it. The conductive heat transfer due to immediate drop/wall contacts is taken

into account with the help of the Mastanaiah–Ganic model [9]. In the present study, a three-stage mechanism of heat transfer in the two-phase flow is considered:

(1) the heat supplied to the wall is being transferred to the drops deposited onto the wall surface and is subsequently spent on their evaporation;
(2) the heat supplied to the wall is being transferred to the gas–vapor–drop mixture;
(3a) some fraction of the heat from the vapor–gas mixture is being transferred to liquid drop to be subsequently spent on their heating and evaporation;
(3b) the remaining part of the heat is spent on heating the gas phase.

The volume fraction of the liquid phase is small ($Z_L < 10^{-4}$), and the drops are rather fine (diameter $d_l < 100$ μm). In each cross section of the duct, all particles are of the same size. Such conditions can be realized due to an intense turbulent mixing between the flow and particles along the duct radius. The drops are uniformly distributed along the duct volume, the latter condition being fulfilled in the whole flow region. In the zone where a complete evaporation of drops occurs, their numeric concentration is modeled with zero-diameter particles. In the flow, the particles suffer no coalescence or fractionation. The Weber number built on the difference between the velocities of the phases and on the drop diameter, $We = \rho|U - U_L|^2 d_l/\sigma \ll 1$, is much smaller than the critical Weber number $We_C \approx 7$ for the data reported in [9]. The drops are treated as rigid spheres. According to the data reported in [1], at volume concentrations of the dispersed phase in the two-phase flow $Z_L < 0.1\%$, the back action of the drops on the structure of the turbulent flow and the inter-drop collisions may be ignored. The drop temperature is uniform along the drop radius [11].

The momentum-, energy-, and mass transfer processes in the gas–drop flow are modeled within the framework of the particle-source-in cell (PSI-Cell) model [20]. The model rests on a hypothesis that liquid drops act as internal sources of vapor mass, momentum, and energy in the gas phase. The mixture gives off heat to the drops; the gas released during this process gets heated to the temperature of the main vapor–air flow and diffuses into the regions with lower vapor content. The heat transfer from the vapor–gas phase to the drops is due to thermal conductivity and convection. The PSI-Cell model allows one to take into account complex processes proceeding with participation of the two phases, these processes being typical for all multi-phase flows.

In the inlet cross section of the duct, the distributions of the temperatures and velocities of the phases are uniform. All drops at the inlet to the duct are of the same size and have identical temperatures. The temperatures of the phases at the duct inlet could be assumed either identical (equilibrium), or different (non-equilibrium regime).

3. Mathematical model

3.1. System of governing equations and model of turbulence

Under the adopted assumptions, the dynamics and heat and mass transfer of the two-phase flow obey a system of differential axial symmetric flow equations. The continuity equation and the equations for the longitudinal velocity U, temperature T of the vapor–gas mixture, and mass concentration K_V of the vapor in the binary vapor–gas mixture, written in the boundary layer approximation, have the following form:

$$\frac{\partial U}{\partial x} + \frac{1}{r}\frac{\partial (rV)}{\partial r} = \frac{JnF}{\rho}$$

$$\rho\left(U\frac{\partial U}{\partial x} + V\frac{\partial U}{\partial r}\right) = -\frac{\partial P}{\partial x} + \frac{\rho}{r}\frac{\partial}{\partial r}\left[r(\mu + \mu_T)\frac{\partial U}{\partial r}\right] - C_D n\rho(U - U_L)|U - U_L|A$$

$$\rho C_p\left(U\frac{\partial T}{\partial x} + V\frac{\partial T}{\partial r}\right) = \frac{1}{r}\frac{\partial}{\partial r}\left[r\left(\frac{\mu}{Pr} + \frac{\mu_T}{Pr_T}\right)\frac{\partial T}{\partial r}\right] - \alpha nF(T - T_L) + \rho D_T\frac{\partial K_V}{\partial r}C_{pV} - C_{pA}\frac{\partial T}{\partial r}$$

$$\rho\left(U\frac{\partial K_V}{\partial x} + V\frac{\partial K_V}{\partial r}\right) = \frac{\rho}{r}\frac{\partial}{\partial r}\left[r\left(\frac{\mu}{Sc} + \frac{\mu_T}{Sc_T}\right)\frac{\partial K_V}{\partial r}\right] + JnF$$

$$\rho = \frac{(1 - Z_L)P}{\Re T}. \quad (1)$$

The continuity equation and the energy and diffusion equations contain source and sink terms that model the influence of liquid drops on the transfer processes, and the equation of motion includes an additional term that takes the dynamic interaction between the phases into account.

In the present study, to determine the turbulent viscosity of the gas phase, the LRN E–ε model of turbulence by Nagano and Tagawa (NT) was used [15]. This modification of the widely used E–ε model was chosen considering the fact that, for ducted flows, this model provides a better agreement with experimental data on turbulent characteristics of the phase-carrier and with heat transfer data. The transfer equations for the kinetic energy of turbulence E and its dissipation rate ε, modified to the case of flows with liquid drops [16,17], have the following form:

$$\rho\left(U\frac{\partial E}{\partial x} + V\frac{\partial E}{\partial r}\right) = \frac{\rho}{r}\frac{\partial}{\partial r}\left[r\left(\mu + \frac{\mu_T}{\sigma_k}\right)\frac{\partial E}{\partial r}\right] + G_k - \rho\varepsilon - S_k$$

$$\rho\left(U\frac{\partial\varepsilon}{\partial x}+V\frac{\partial\varepsilon}{\partial r}\right)=\frac{\rho}{r}\frac{\partial}{\partial r}\left[r\left(\mu+\frac{\mu_{\mathrm{T}}}{\sigma_{\varepsilon}}\right)\frac{\partial\varepsilon}{\partial r}\right]+\frac{C_{\varepsilon1}\varepsilon f_1 G_k}{E}-\frac{C_{\varepsilon2}\varepsilon^2\rho f_2}{E}-S_{\varepsilon},\qquad(2)$$

where S_k is the term that takes into account the additional dissipation of turbulence energy due to relatively small particles (the dynamic slip in the mean motion is negligible):

$$S_{\mathrm{E}}=\frac{2M_{\mathrm{L}}E}{\tau}\exp(-\Omega^{\mathrm{L}}/\tau),$$

and S_ε is the term that takes into account the influence of relatively small particles on the rate of dissipation of turbulence energy (the dynamic slip in the mean motion is negligible):

$$S_{\varepsilon}=\frac{2M_{\mathrm{L}}\varepsilon}{\tau}\exp(-\Omega^{\varepsilon}/\tau).$$

The dynamic viscosity of the gas phase may be calculated in the framework of the standard two-equation model:

$$\mu_{\mathrm{T}}=C_{\mu}f_{\mu}\rho E^2/\varepsilon.$$

The constants and damping functions coincides with the corresponding values adopted in the model of turbulence [15]

$$C_{\mu}=0.09,\ \sigma_k=1.4,\ \sigma_{\varepsilon}=1.3,\ C_{\varepsilon1}=1.45,\ C_{\varepsilon2}=1.9,$$

$$f_1=1,\ f_2=[1-\exp(-y_+/6)]^2\left[1-0.3\exp\left\{-\left(Re_{\mathrm{T}}^{3/4}/6.5\right)^2\right\}\right],$$

$$G_k=\mu_{\mathrm{T}}\left(\frac{\partial U}{\partial r}\right)^2,\ f_{\mu}=[1-\exp(-y_+/26)]^2(1+4.1/Re_{\mathrm{T}}^{3/4}).$$

The dependence for determining the derivative $\partial P/\partial x$ in the equation of flow over the initial length of the duct may be represented in the form

$$-\frac{\partial P}{\partial x}=\rho U_0\frac{\partial U_0}{\partial x}.$$

The change in the flow velocity in the undisturbed core of the flow may be found from the condition of constancy of the mass flux in the duct:

$$\rho U_0\pi(R-\delta)^2+2\rho\pi\int_{R-\delta}^{R}Ur\,\mathrm{d}r=G_1+G_{\mathrm{E}},\qquad(3)$$

where G_1 and G_{E} are respectively the mass flux of the mixture in a duct cross section and the mass flux due to vapor formation. The formulas for G_1 and G_2 in (3) are

$$G_1=\rho U_{\mathrm{m}}\pi R^2(M_{\mathrm{A}}+M_{\mathrm{V}});$$

$$G_{\mathrm{E}}=\rho_{\mathrm{V}}U_{\mathrm{m}}\pi R^2(M_{\mathrm{V}i}-M_{\mathrm{V}i-1}).$$

The final expression for the flow velocity at the duct axis U_0 is

$$U_0=\left(G_1+G_{\mathrm{E}}-2\rho\pi\int_{R-\delta}^{R}Ur\,\mathrm{d}r\right)\Big/\left[\rho\pi(R-\delta)^2\right].\qquad(4)$$

Relations (1) should be supplemented with the energy-balance equation for a drop

$$C_{p\mathrm{L}}U_{\mathrm{L}}m\frac{\partial T_{\mathrm{L}}}{\partial x}=\alpha F(T-T_{\mathrm{L}})-JF[L+C_{p\mathrm{V}}(T-T_{\mathrm{L}})]\qquad(5)$$

and with the equation of vapor-mass conservation at the evaporating surface of a drop [21]

$$J=JK_{\mathrm{V}}^{*}-\rho_{\mathrm{V}}D\frac{K_{\mathrm{V}}^{*}}{\partial r}.\qquad(6)$$

Here m is the drop mass.

Taking into account that the diffusional Stanton number St_{D} is

$$St_{\mathrm{D}}=-\rho_{\mathrm{V}}D\frac{\partial K_{\mathrm{V}}^{*}}{\partial r}/\rho U(K_{\mathrm{V}}^{*}-K_{\mathrm{V}}),$$

we may write equation of mass conservation (6) in the form

$$J=St_{\mathrm{D}}\rho Ub_{1\mathrm{D}},\qquad(7)$$

where

$$b_{1\mathrm{D}}=(K_{\mathrm{V}}^{*}-K_{\mathrm{V}})/(1-K_{\mathrm{V}}^{*})\qquad(8)$$

is the diffusional injection parameter. The concentration of vapor at the evaporating surface of a drop K_{V}^{*} is related with the drop temperature T_{L} by the saturation curve.

The equations of heat and mass transfer from the surface of a non-evaporating drop have the form [16]

$$Nu_{\mathrm{P}}=\alpha_{\mathrm{P}}d/\lambda=2+0.6Re_{\mathrm{L}}^{1/2}Pr^{1/3}\quad\text{and}$$

$$Sh_{\mathrm{P}}=\beta d/D=2+0.6Re_{\mathrm{L}}^{1/2}Sc^{1/3}.$$

Here $Re_{\mathrm{P}}=\rho d_{\mathrm{P}}\sqrt{(U-U_{\mathrm{P}})^2+(V-V_{\mathrm{P}})^2}/\mu$—Reynolds number of non-evaporating particle built on the slip velocity of the phases.

The diffusional Stanton number may be determined from the expression [21]

$$St_{\mathrm{D}}=Sh_{\mathrm{P}}/(Re_{\mathrm{L}}Sc),$$

and then Eq. (6) re-arranges to

$$J=(2+0.6Re_{\mathrm{L}}^{1/2}Sc^{1/3})\rho Ub_{1\mathrm{D}}/(Re_{\mathrm{L}}Sc).\qquad(9)$$

According to [22], the heat transfer coefficient of evaporating drops α is related to the analogous coefficient of non-evaporating drops α_{P} by the formula

$$\alpha=\alpha_{\mathrm{P}}/[1+C_p(T-T_{\mathrm{L}})/L].\qquad(10)$$

The material balance equation for the binary vapor–air mixture is

$$K_{\mathrm{A}}+K_{\mathrm{V}}=1.$$

For the triple vapor–gas–liquid mixture, this equation may be written as

$$M_A + M_V + M_L = 1. \tag{11}$$

The relation between the mass concentrations of the mixture components, K and M, is given by the formulas

$$K_V = M_V/(M_A + M_V) \quad \text{and}$$
$$K_A = M_A/(M_A + M_V) = 1 - K_V.$$

The expression for the current drop diameter in the ith calculation cross-section is [12]

$$d_i^3 = d_{i-1}^3 - Jd_{i-1}^2 \frac{6\Delta x}{\rho_L U_{mi}}. \tag{12}$$

In accord with (12), the choice of U_{mi} as a characteristic flow velocity was motivated by the fact that the adopted model implies an intense mixing of particles over the duct radius, which provides for radial uniformity of drop sizes across the duct.

In flows with intense evaporation, the gas phase velocity increases in the downstream direction due to vapor generation. This phenomenon is allowed for by the source term in the continuity equation, the increase in the local velocities over the duct cross section being dependent on the distribution of the gas phase temperature. The mean-flow velocity of the vapor–gas mixture in a current duct cross-section with allowance for the vapor-mass income from evaporating drops was calculated from the formula

$$U_{mi} = \frac{U_{mi-1}}{1 - n\rho_L(d_i^3 - d_{i-1}^3)/\rho}.$$

In the present study, the Prandtl and Schmidt numbers were assumed to be uniform both over the duct length and over duct radius, and equal to $Pr_T = Sc_T = 0.9$.

3.2. A model for drop precipitation onto the duct wall from a two-phase flow, and heat transfer between a precipitated drop and the wall

To predict the rate of deposition of liquid drops onto the wall from the turbulent flow, the following theoretical dependence previously proposed was used [23]:

$$k_{L+} = \frac{0.115/(B^{0.75}\tau_+^{3/8}) + 2.5 \times 10^{-4}\tau_+^{2.5}}{1 + 10^{-3}\tau_+^{2.5} + 1.25 \times 10^{-3}\tau_+^3/\sqrt{R_+}}. \tag{13}$$

Here $B = 12.73\sqrt{\rho/\rho_L}\pi\nu^3/(1.381 \times 10^{-23} TU_*)$ is a factor that takes into account the influence of Brownian diffusion on drop precipitation [23].

To determine the mass concentration of particles deposited onto the duct wall M_{LW} from the turbulent gas–vapor–drop flow, we use the following algebraic relations.

The mass of the liquid deposited onto the duct wall is

$$m_W = J_W \Delta x 2\pi \Delta r \Delta t,$$

where $J_W = k_L\rho_L$ is the mass rate of precipitation of the drops, Δx and Δr are the steps along the longitudinal and transverse coordinates, and Δt is time.

The total number of deposited drops is

$$N_W = \frac{m_W}{\rho_L \pi d^3/6}.$$

The numeric concentration of the dispersed phase in the flow of particles to be deposited onto the duct wall is

$$n_W = \frac{N_W}{\pi R^2 \Delta x},$$

$n = n_{i-1} - n_W$ is the current numeric concentration of the particles which have remained in the flow, and $i - 1$ is the index that corresponds to the previous nodal point.

The mass concentration of drops precipitated on the wall surface is

$$M_{LW} = \frac{n_W \rho_L \pi d^3}{6\rho}. \tag{14a}$$

During the precipitation of the particles onto the wall, some portion of the heat flux supplied to the wall is spent on their evaporation. As in many previous models, for instance in the model used in [9], here we assume that the superposition principle may be applied to the heat flows under consideration. The heat-flux density q_W of the heat flow supplied to the duct wall includes the components corresponding to the heat flows from the wall to drops q_{WL} and from the wall to the vapor–gas–drop mixture q_{WF}.

The heat flux density from the duct wall to drops for $T_W > T_L$ has the form [9]

$$q_W = \exp[1 - (T_W/T_L)^2] J_W L M_{Lm}. \tag{14b}$$

The mean-mass concentration of liquid drops obtained by averaging their local concentrations over the duct cross section is given by the expression

$$M_{Lm} = \frac{2}{U_m R^2} \int_0^R M_L U r \, dr.$$

3.3. Equation of particle motion

All computations in the present study were performed for a vertically oriented duct. In this case, the following forces acting on the particles were considered: resistance force, gravitational force, and Archimedean force. The Saffman and Magnus forces were ignored in the present study. The aerodynamic forces due to pressure gradient, attached mass, and Basse effect are assumed to be negligible since these forces are propor-

tional to the gas/liquid density ratio, which, in most practical cases, are of the order of $\sim 10^{-3}$.

The equation of drop motion with allowance for the skin-friction, gravitational, and buoyancy forces may be written, in their vector form, as

$$m\frac{\mathrm{d}\vec{U}_\mathrm{L}}{\mathrm{d}t} = C_\mathrm{D}\rho(\vec{U}-\vec{U}_\mathrm{L})|\vec{U}-\vec{U}_\mathrm{L}|A + m\vec{g}(1-\rho/\rho_\mathrm{L}), \tag{15a}$$

where C_D is the coefficient of aerodynamic resistance and g is the free-fall acceleration.

Projections of this equation onto the x- and r-axes have the following form. For the longitudinal, x-direction, we have:

$$m\frac{\mathrm{d}U_\mathrm{L}}{\mathrm{d}t} = C_\mathrm{D}\rho(U-U_\mathrm{L})|\vec{U}-\vec{U}_\mathrm{L}|A \pm mg(1-\rho/\rho_\mathrm{L}).$$

For the radial, r-direction:

$$m\frac{\mathrm{d}V_\mathrm{L}}{\mathrm{d}t} = C_\mathrm{D}\rho(V-V_\mathrm{L})|\vec{V}-\vec{V}_\mathrm{L}|A.$$

The aerodynamic coefficient of resistance for evaporating drops C_D is given by the expression [16]

$$C_\mathrm{D} = \frac{C_\mathrm{DP}}{1+C_p(T-T_\mathrm{L})/L}.$$

Here C_DP is the coefficient of resistance of non-evaporating drops, given by the formulas

$$C_\mathrm{DP} = \begin{cases} 24/Re_\mathrm{L} \text{ при } Re_\mathrm{L} \leqslant 1, \\ \dfrac{24}{Re_\mathrm{L}}(1+Re_\mathrm{L}^{2/3}/6) \text{ при } Re_\mathrm{L} > 1. \end{cases}$$

To compare theoretical predictions with experimentally measured gas phase and drop velocity pulsations, we had to compute these quantities in our numerical simulations. Here, the particles were assumed to be sufficiently large and their dynamic relaxation time τ longer than the Eulerian integral time scale Ω^E of the turbulence. The integral time scale Ω^E which was necessary for determining the transverse component of gas phase pulsations, is given by the formula [23]

$$\Omega^\mathrm{E}_+ = \Omega^\mathrm{E}U_*^2/\nu = \sqrt{l_{0+}^2 + l_+^2},$$

which for $y_+ \to 0$ reduces to the relation $\Omega^\mathrm{E}_+ = l_{0+} \approx 10$ (within the viscous sublayer, the integral time scale of turbulence is assumed to be a constant value) and in the turbulent flow core to the relation $\Omega^\mathrm{E}_+ = l_+ = lU_*/\nu$ where l_+ is the relative mixing length and l is the mixing length given by the Prandtl–Nukuradze formula [24]

$$l = R[0.14 - 0.08(r/R)^2 + 0.06(r/R)^4].$$

The radial component of the root-mean-squared pulsations of the gas phase flow is given by the formula [24]

$$\langle v^2\rangle = v_\mathrm{T}/\Omega^\mathrm{E}Sc_\mathrm{T}. \tag{15b}$$

The amplitude of the root-mean-squared pulsations of the phase-carrier in the longitudinal direction is [24]

$$\langle u^2\rangle \approx 1.3E. \tag{16}$$

For sufficiently large particles, the turbulence intensity of the dispersed phase may be related to the amplitude of root-mean-square pulsations of the gas phase and to the time of dynamic relaxation of the particles by the following formulas, previously used in [25]:

$$\langle v_\mathrm{L}^2\rangle = \langle v^2\rangle\frac{\Omega^\mathrm{E}}{\tau}; \quad \Omega^\mathrm{E} = \frac{\Gamma^\mathrm{E}}{\sqrt{\langle v^2\rangle}}; \quad \Gamma^\mathrm{E} = 0.14R, \tag{17}$$

where Γ^E is the geometric turbulence scale of the phase-carrier.

The relation between the time turbulence scales is [25]

$$\Omega^\mathrm{L} \approx 0.61\Omega^\mathrm{E}.$$

3.4. Boundary and inlet conditions

At the duct axis and at the outer border of the boundary layer, the following symmetry conditions were posed

$$\frac{\partial T}{\partial r} = \frac{\partial K_\mathrm{V}}{\partial r} = \frac{\partial U}{\partial r} = \frac{\partial E}{\partial r} = \frac{\partial \varepsilon}{\partial r} = V = 0 \quad \text{at } r = 0 \quad \text{and} \quad r = \delta. \tag{18}$$

At the wall (at $r = R$), no-slip conditions for the gas phase velocity are fulfilled:

$$U = V = 0,$$

as well as the condition of wall impermeability for the flow of substance

$$\left(\frac{\partial K_\mathrm{V}}{\partial r}\right)_\mathrm{W} = 0$$

and the Fourier heat transfer law

$$-\lambda\frac{\partial T}{\partial r} = q_\mathrm{WF}.$$

In the adopted model of turbulence, the following conditions were set:

$$E = 0, \quad \varepsilon_W = \nu\left(\frac{\partial^2 E}{\partial r^2}\right)_W.$$

In the inlet cross section of the duct,

$$U = U_1, \quad V = V_1, \quad T = T_1, \quad M_\mathrm{L} = M_\mathrm{L1}, \quad T_\mathrm{L} = T_\mathrm{L1}, \quad d = d_1, \quad K_\mathrm{V} = K_\mathrm{V1}, \quad E = E_1, \quad \text{and} \quad \varepsilon = \varepsilon_1. \tag{19}$$

In the present study, the degree of gas phase turbulence at the duct inlet was assumed to equal $Tu = \sqrt{1/3(\langle u^2\rangle + \langle v^2\rangle + \langle w^2\rangle)}/U = 3\%$.

Relations (1)–(17) with appropriate boundary and initial conditions (18) and (19) represent a closed system of equations for heat and mass transfer processes in a turbulent two-phase flow which allow one to calculate all quantities of interest (distributions of temperature, concentrations of phases, and components of the vapor–gas mixture) and predict the evolution of particle sizes.

3.5. Numerical realization

The numerical solution of the partial differential conditions was obtained with the help of the Crank–Nicholson finite-difference scheme [26] by transforming the initial differential equations in a system of discrete algebraic linear equations. The obtained three-diagonal system was solved by the sweep method using the Thomas algorithm described in more details elsewhere [26]. To spatially resolve the fine structure of the near-wall turbulent flow, we used a computation grid with a variable mesh size. The mesh size was decreasing towards the duct wall and constant in the longitudinal direction.

Since the mesh size in the transverse direction was variable, for the sake of convenience the coordinate r was transformed so that the equations could be solved on a spatially uniform computation grid in the whole computation domain. For the boundary layer problem of interest, the most appropriate transformation of coordinates was proposed in [26].

All computations were performed on a grid with 201 nodal points in the longitudinal direction and 101 such points in the transverse direction. Besides, some methodical computations were performed on a finer computation grid (201 and 201 nodal points along the duct length and radius, respectively). Further increase in the total number of nodal points was found to cause no substantial changes in the calculation results.

Since system (1)–(17) included non-linear equations, to solve it, an iteration algorithm was used. The following convergence conditions were adopted: $|Y_i - Y_{i-1}| < 10^{-4}$, where Y stands for U, E, ε, T, K_V or T_L. The computations were terminated on meeting all these criteria.

4. Testing of the model

4.1. Single-phase flow mode

In the framework of the present study, the calculations according to the adopted E–ε model of turbulence were tested by comparing their results with the DNS data and with the PIV and LDA data previously reported for a ducted isothermal single-phase air flow in [27]. In addition, the data gained in the present study were found to perfectly comply with heat transfer regularities revealed for a turbulent single-phase gas flow in [21].

4.2. Two-phase flow mode. Hydrodynamics of the flow

For a comparative analysis of data gained for a two-phase flow, experimental data obtained by Varaksin and Polyakov [28] for a descending flow of a gas/glass particles mixture and experimental data obtained by Cramer and Depew [29] for an ascending gas/glass particles flow were used. The predicted and measured distributions of the particle Reynolds number $Re_P = d\Delta U/v$ along the duct radius are shown in Fig. 1.

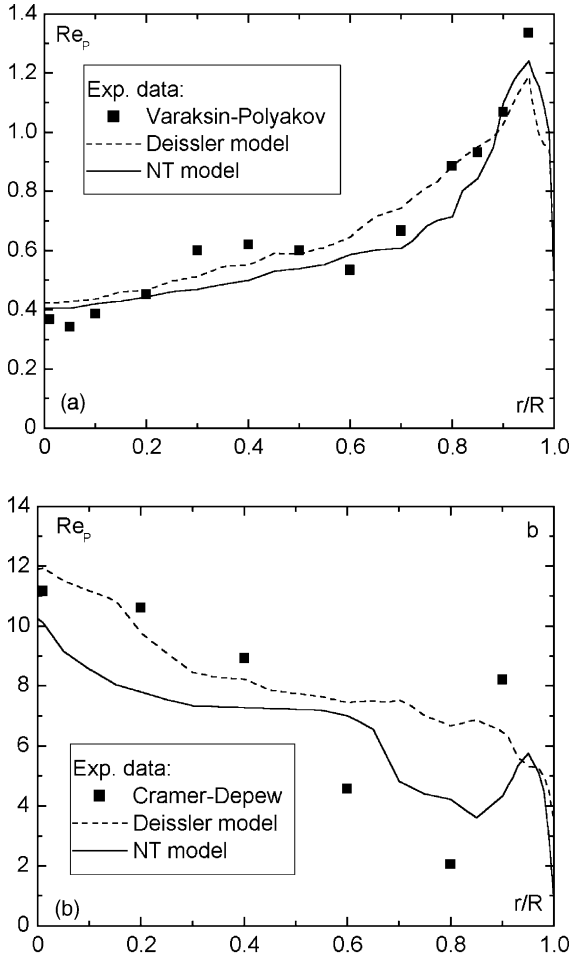

Fig. 1. Radial distributions of measured and calculated Reynolds numbers of glass particles in the duct with a stabilized flow. Solid curves [15]; dotted curves [14]. (a) Experimental data of [28] for a descending flow; (b) experimental data of [29] for an ascending flow.

The initial data for the numerical experiment for the conditions of [28] were the following: $2R = 46$ mm, $Re = 12\,300$, $U_0 = 4$ m/s, $M_P = 2\%$, $d_P = 50$ μm, $\rho_p = 2550$ kg/m^3, and $\tau_+ = 79$. The initial data for the conditions of [29] were $2R = 12.7$ mm, $Re = 24\,500$, $U_0 = 28.7$ m/s, $M_P = 26\%$, $d_P = 62$ μm, $\rho_p = 2640$ kg/m^3, and $\tau_+ = 5417$.

In the calculations, the algebraic Deissler model of turbulence [14] and the E–ε model of turbulence [15] were used.

Inspection of data in Fig. 1a for a two-phase flow of a mixture with a low concentration of the dispersed phase shows a good agreement between the data predicted by both models of turbulence and measured values over the whole duct volume. Both the calculation and experimental data shows that the slip velocity of the phases increases in the near-wall zone of the descending flow.

Just the opposite pattern of slip velocity (see Fig. 1b) is displayed by the ascending flow of the suspension of glass particles. The maximum and minimum values of the slip velocity were observed at the duct axis and near the duct wall, respectively.

It is hardly possible to conclude definitely from the data shown in Fig. 1b which of the two models of turbulence more adequately predicts the behavior of particle Reynolds number Re_L in the flow with a high concentration of the liquid phase. It should be noted that the concentration of the dispersed phase for the data shown in Fig. 1b is an order of magnitude higher than that in Fig. 1a. This could be the reason for the observed difference between the predicted and measured values. In a flow with a high mass concentration, effects due to inter-particle and particle-wall collisions, and also due to possible rotation of the dispersed phase, may exert a substantial influence on the flow pattern [16]. Nevertheless, the satisfactory agreement between the data predicted by the two models and experimental results for the paraxial flow region is worth noting. For the near-wall region, the NT model predicts an increase in Re_L, whereas the Deissler model yields no such increase.

It should be noted that both the NT and Deissler models, as applied to ascending or descending flows yield results being in qualitative agreement with the LES data [30] gained for a vertical isothermal dispersion flow in a duct.

The distributions of relative axial and radial pulsating velocities of the gas and dispersed phases along the duct radius are compared in Fig. 2 with the experimental data of [31]. The tests were performed for a descending flow of an air/glass particles flow with the help of LDA. The initial data for the numerical experiment for the conditions of [35] were the following: $2R = 46$ mm, $U_0 = 5.2$ m/s, $d_P = 50$ μm, $\rho_p = 2550$ kg/m^3, $M_P = 5\%$, $\tau_+ = 125$, and $Re = 15\,300$.

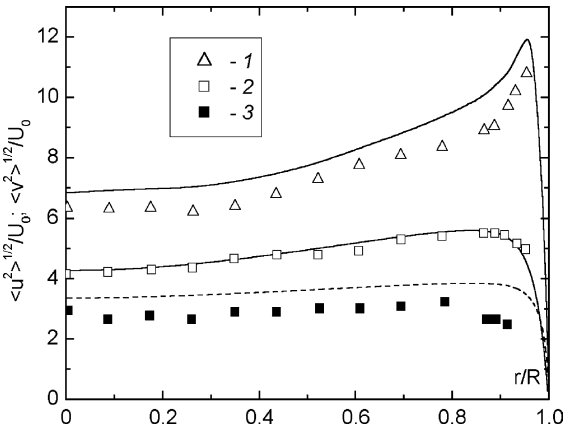

Fig. 2. Comparison between the predicted and measured [31] root-mean-square pulsations of air and glass-particle flows. (1) $\langle u^2\rangle^{1/2}/U_0$; (2) $\langle v^2\rangle^{1/2}/U_0$; (3) $\langle v_L^2\rangle^{1/2}/U_0$. Curves—calculation data.

The following conclusions can be drawn from the comparative analysis. The predicted values of the pulsating velocity of the gas phase in the transverse and longitudinal directions rather adequately describe the experimental data. The pulsational velocity of the particles calculated according to the Derevich model for inertial particles [25] fairly well agrees with the experimental data. Note that the calculation data show a better agreement with the measured amplitude of transverse pulsations compared to the longitudinal pulsations of the phase-carrier velocity. It is seen from the distributions shown in Fig. 2 that the intensity of longitudinal pulsations of the particle velocity is lower than that for the phase-carrier. This fact can be explained as follows. The Stokes number in the large-scale pulsational motion is defined as $\mathrm{Stk} = \tau/\Omega^L$, being for the conditions under consideration of the order of unity ($\mathrm{Stk} \approx 1$), from which it follows that particles readily get involved into the large-scale pulsational motion and take off energy from the turbulent phase-carrier vortices. A decrease in the intensity of the transverse pulsations of the gas phase leads to a decrease of the velocity pulsations of the particles [31].

Fig. 3 compares the numerical and experimental data by Varaksin et al. [32] on the radial distributions of the kinetic energy of gas phase turbulence for various concentrations of glass particles. The conditions of the selected experiments correspond to the following values of determining parameters: $2R = 64$ mm, $U_0 = 6.4$ m/s, $d_P = 50$ μm, $\rho_p = 2550$ kg/m^3, $\tau_+ = 20$, and $Re = 25\,600$. It is seen from Fig. 4 that relatively small particles present in the flow suppress the turbulence. The laminarizing action of these particles increases with increasing mass concentration of particles; it also increases with distance from the wall. These data are in a good qualitative agreement with the experimental data of [33].

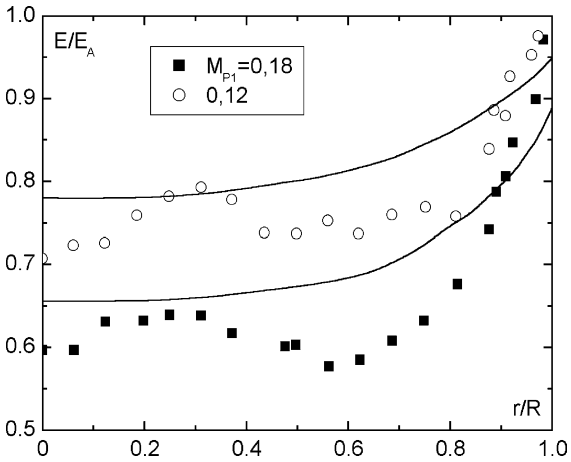

Fig. 3. Impact of particles on the distribution of the gas phase turbulence energy over the duct cross section. Curves—calculation data, points—experimental data [32].

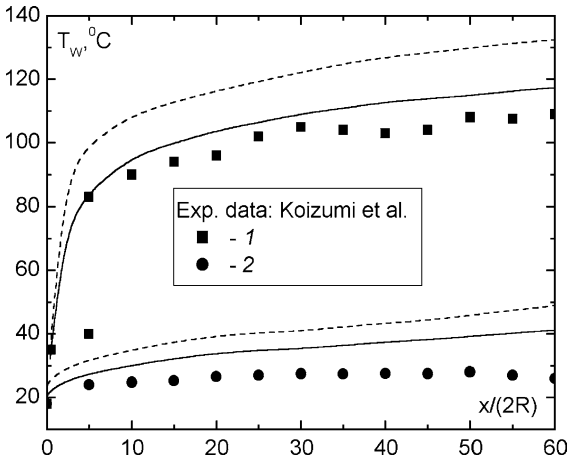

Fig. 4. Variation of the wall temperature along the duct length in a single-component vapor–drop flow. Solid curves [15]; dotted curves [14]; points—experimental data of [7]. (1) $M_{L1} = 0.35$, $q_W = 7.14$ kW/m^2; (2) $M_{L1} = 0.43$, $q_W = 2.13$ kW/m^2.

4.3. Two-phase flow mode. Heat transfer

To estimate the prediction accuracy for the rate of heat transfer in a vapor–drop flow, we compared the results obtained in the present study with the experimental data by Koizumi et al. [7]. The wall-temperature profile over the duct length for a vapor–drop flow is shown in Fig. 4. The initial data for the comparative analysis were the following: duct diameter 10 mm, saturation pressure $P = 3.08 \times 10^5$ Pa, $T_l = T_{L1} = T_l = 300$ K, $d_l = 30$ μm, inlet Reynolds number $Re_l = U_l 2R/\nu = 5.1 \times 10^5$, the working liquid—Freon R-113. As is seen from Fig. 5, the predicted and measured data agree better with each other at high thermal loads than at low

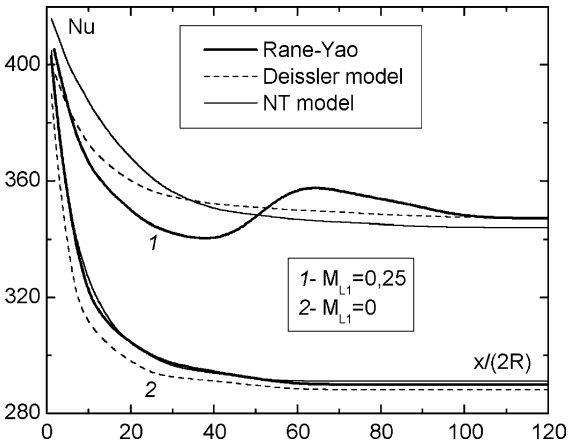

Fig. 5. Comparison of the calculation results according to models [14] and [15] with the data of [8] on heat transfer in a turbulent vapor–drop flow. $Re_l = 1.6 \times 10^5$.

values of q_W. A possible reason for the difference between the predicted and measured data is inconsistency between the adopted and actual mechanisms of heat transfer between the gas–drop flow and the wall. In particular, as the wall temperature decreases, the formation of a liquid film on the wall surface becomes more probable. As was mentioned previously, the present model ignores this phenomenon. Simultaneously, the E–ε model provides a better agreement with the experimental data compared to the algebraic Deissler model.

The validity of the developed computational model was tested by comparing the predicted heat transfer data with numerical simulations of heat transfer in turbulent stabilized vapor–drop flows [8] (see Fig. 5). A satisfactory agreement between the predictions of the Deissler [14] and NT [15] models, on the one hand, and the data of [8] on the other was obtained; it should be mentioned however that the results yielded by the NT model compare better with the calculations by Rane–Yao [8] than the data gained with the algebraic model [14].

From the analysis of the data shown in Figs. 1–5, the following conclusion can be drawn. The E–ε model and the algebraic relations for the root-mean-squared pulsations of the gas phase and particles rather accurately predicts the pulsational processes, the dynamics of the motion of the gas and dispersed phases, and heat transfer regularities observed for developed two-phase flows.

All subsequent calculations were performed using the E–ε model.

5. Calculation results on heat transfer in a ducted gas–vapor–drop flow and their comparison with available experimental and numerical data

The calculations were performed for a flow of an air/water vapor mixture with water drops (under atmo-

spheric pressure). The duct length was 2 m, and the inner duct diameter 0.02 m. The ranges of initial parameters were the following: inlet temperature of the vapor–gas mixture $T_1 = 293$–373 K; flow Reynolds number $Re = U_1 2R/\nu = 5 \times 10^3$–$10^6$; drop diameter at the duct inlet $d_1 = 0.1$–100 μm, which corresponds to a dimensional relaxation time of the liquid drops $\tau_+ = 10^{-3}$–10^3; mass fraction of the drop phase $M_{L1} = 0$–0.1; and mass fraction of air $M_{A1} = 0$–0.8. All calculations were performed for a constant wall heat-flux density ($q_W = \text{const}$), namely, for $q_W = 1$ kW/m^2.

Fig. 6 illustrates the effect of mass concentration of liquid drops in the flow on the skin friction. As is seen, the skin friction almost linearly increases with increasing concentration of particles. However, this increase is insignificant, amounting to about 10% for large particles available in the flow in the mass concentration $M_{L1} = 0.1$.

One more important feature in Fig. 6 deserves mention. With increasing particle diameter, the skin friction also increases. The profile of axial velocity and, hence, skin friction are affected by a number of factors. The evaporation of liquid drops leads to an increase in the local flow velocity, and the dispersed phase suppresses the gas phase turbulent pulsations. This is evident from Fig. 7, where a larger particle size and a higher concentration of large particles cause more appreciable laminarization of the flow. The decrease in the turbulence kinetic energy is due to active involvement of relatively small particles into the pulsational flow of the gas phase and due to the fact that the vapor–gas mixture gives over some part of its pulsational energy to these particles. These conclusions are in qualitative agreement with the experimental data obtained in [33], where it was

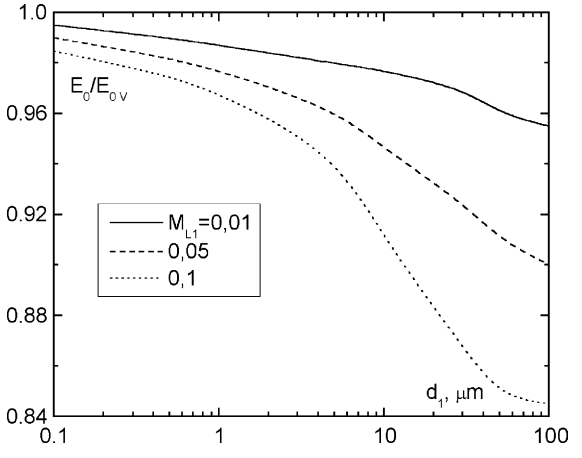

Fig. 6. Skin friction versus the mass concentration of the liquid phase. $Re = 13000$; $x/(2R) = 20$; $T_1 = 373$ K; $q_W = 1$ kW/m^2. (1) $d = 1$ μm, $\tau_+ = 0.1$; (2) $d = 10$ μm, $\tau_+ = 8$; (3) $d = 30$ μm, $\tau_+ = 70$; (4) $d = 50$ μm, $\tau_+ = 190$; (5) $d = 100$ μm, $\tau_+ = 760$.

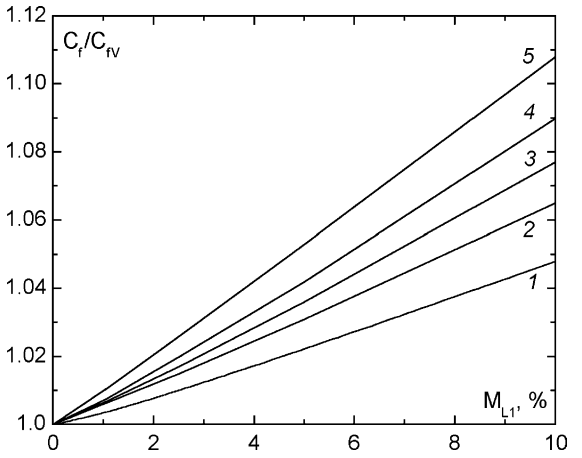

Fig. 7. Gas phase turbulence energy of the gas–vapor–drop flow versus the initial drop diameter. Conditions are the same as in Fig. 6.

established that addition of large particles ($d_P = 3$ mm) to the flow results in an increase of its turbulence level, whereas addition of fine particles ($d_P = 200$ μm) or a substantial decrease of their density (from $\rho_P = 2600$ kg/m^3 to $\rho_P = 1000$ kg/m^3) lead to an increase in the kinetic turbulence energy. At the same time, a third factor, acceleration of more inertial particles by the flow, may exert a more pronounced effect and, finally, cause an increase in the skin friction with increasing drop diameter. However, this point deserves a more detailed numerical and experimental study.

Fig. 8 shows the heat transfer intensification ratio as a function of the mass concentration of liquid drops in a gas–vapor–drop flow. Here Nu_V is the Nusselt number for a single-phase flow with fixed Reynolds number. As

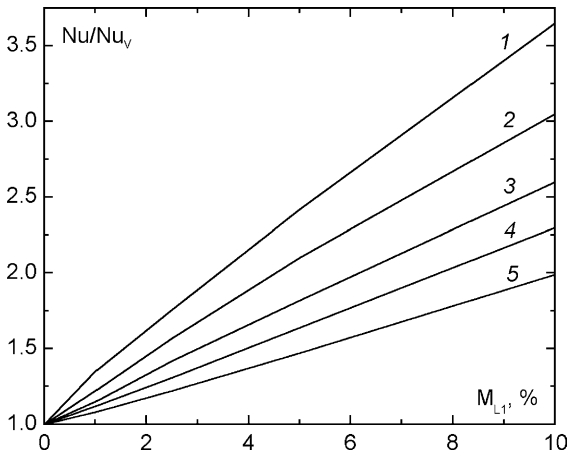

Fig. 8. Variation of the heat transfer intensification ratio Nu/Nu_V in the gas–vapor–drop flow. Labeling of the curves is the same as in Fig. 6.

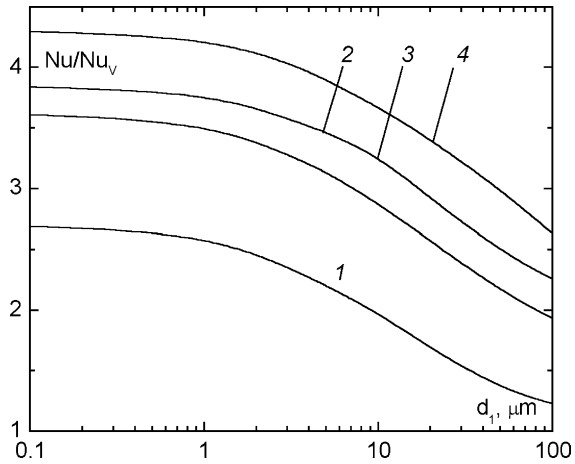

Fig. 9. Heat transfer intensification ratio Nu/Nu_V versus the initial drop diameter. $x/(2R) = 20$. (1) $Re = 1.8 \times 10^3$; (2) 10^4; (3) 5×10^4; (4) 10^5.

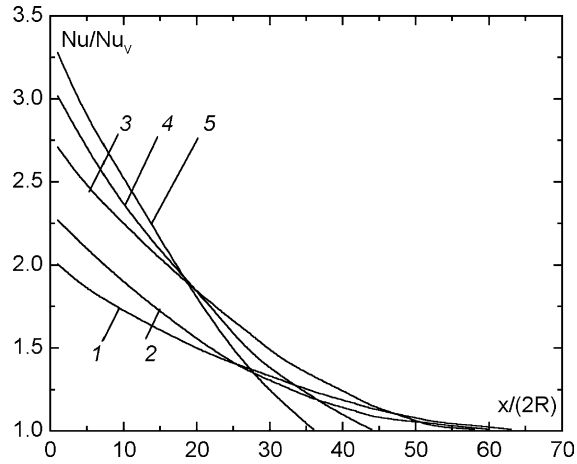

Fig. 10. Heat transfer intensification ratio versus air concentration. $Re = 13\,000$; $M_{L1} = 0.1$. (1) $M_{A1} = 0$; (2) 0.01; (3) 0.1; (4) 0.2; (5) 0.5.

is seen from Fig. 8, the liquid drops exert a substantial influence of the heat transfer intensification ratio in the two-phase gas–vapor–drop flow (the heat transfer rate increases by a factor of 3), whereas the skin friction increases only insignificantly (roughly by 10%). An increase in the initial drop diameter results in an increased skin friction, whereas, as it follows from Fig. 8, the heat transfer rate decreases.

The impact of the drop diameter on the heat transfer intensification ratio is analyzed in more detail in Fig. 9. An increase in the drop diameter (at a fixed mass concentration of the liquid phase) diminishes the intensity of heat and mass transfer processes, which effect can be attributed to an appreciable reduction in the interface area between the particles and the vapor–gas flow. For relatively fine particles ($d_1 < 2$–5 μm), the Nu/Nu_V ratio does not depend on the drop diameter. This range of particle sizes determines a steady-state evaporation regime, with the vapor–gas mixture being in thermodynamic equilibrium with the liquid phase.

Fig. 10 shows the heat transfer intensification ratio as a function of air concentration in the vapor–gas mixture. The Nu/Nu_V ratio is minimal for a single-component vapor–drop flow without air (curve 1). With increasing air concentration, the heat transfer rate increases since the diffusion of vapor from the drop surface becomes more intense; however, in this case the extension of the two-phase flow region in the downstream direction shrinks due to the more intense evaporation.

Such a complex multi-stage mechanism of heat transfer from the wall to the two-phase flow being operative, it is of special interest to determine the individual contributions due to various heat transfer components into the total heat flux at the wall. The distributions of various heat flux components along the duct length for two values of the mass concentration of the liquid phase, $M_{L1} = 0.01$ and 0.1, are shown in Fig. 11, where q_F is the heat spent on heating the vapor–drop flow, q_{WL} is the heat-flux density due to the conductive heat transfer upon immediate drop/wall contacts, q_E is the heat spent on drop evaporation in the flow, and q_L is the heat spent on drop heating. From Fig. 11, the following conclusions can be drawn. Over an initial length of the duct, rather a high fraction of the heat supplied to the duct wall is being spent on conductive heat transfer and evaporation of liquid drops. Further downstream, as the drops undergo evaporation, the components q_L, q_{WL}, and q_E all decrease, whereas the component q_F due to the heat flow to the vapor–gas phase permanently increases until it finally reaches unity. In this case, a

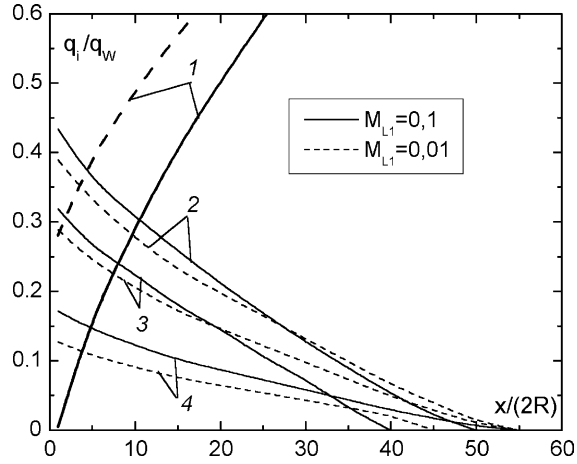

Fig. 11. Distributions of the heat flux components in the two-phase gas–vapor–drop flow. The conditions are the same as in Fig. 6. (1) q_F/q_W; (2) q_{WL}/q_W; (3) q_E/q_W; (4) q_L/q_W.

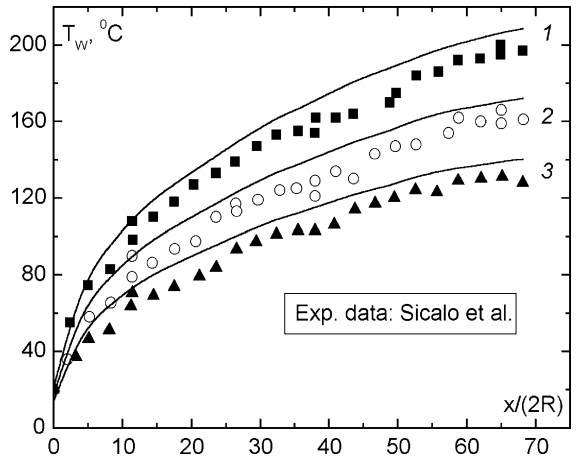

Fig. 12. Wall-temperature profiles. Curves—calculation data; points—experimental data by Sicalo et al. [13]. (1) $q_W = 17.84$ kW/m^2; (2) 13.92; (3) 11.5.

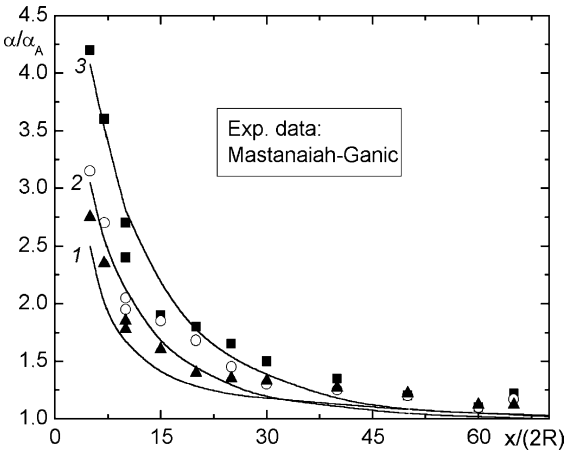

Fig. 13. Comparison of predicted heat transfer intensification ratios with the experimental data of [9]. (1) $q_W = 14.53$ kW/m^2; (2) 8.34; (3) 6.4.

single-phase flow takes place. A change in the inlet concentration of the liquid induces no fundamental differences into the proportions between the various heat transfer components except for the initial flow region, where the concentration M_{L1} is low and a predominant contribution is due to the heat transfer to the vapor–gas mixture.

Subsequent figures compare the calculation results obtained in the present study with some experimental data previously reported in the literature.

The profile of the wall temperature T_W along the duct length, measured in [13], is shown in Fig. 12. The initial data in the comparative analysis were the following: $M_{L1} = 0.5\%$, $Re = U_1 2R/\nu = 39\,300$, $2R = 13.2$ mm, calculation length 0.924 m, $G_A = 7.58$ g/s, $d_l = 16$ μm, $\tau_+ = 272$, and $T_l = 293$ K. The experiments were carried out under atmospheric pressure. Fig. 12 demonstrates a fairly good agreement between that the predicted and measured wall-temperature profiles.

Fig. 13 shows the heat transfer intensification ratios measured in [9] and heat transfer intensification ratios calculated in the present study. Here, the quantity α_A refers to the case of a single-phase air flow with all other conditions kept unchanged. The initial conditions in the numerical experiments were the following: $M_{L1} =$ 1.1–2.1%, $Re = U_1 2R/\nu = 21\,800$–$58\,600$, $2R = 12.95$ mm, computation length 0.889 m, $G_A = 4.02$–10.8 g/s, $d_l = 9$–23 μm, $\tau_+ = 139$–208, and $T_l = 300$ K. The experiments were carried out under atmospheric pressure. Both measured and predicted α/α_A ratios display a monotonic decrease in the downstream direction; they decreases with decreasing wall heat flux density. An increase in the wall heat flux density results in a decreased heat transfer intensification ratio since, in this case, the wall temperature increases.

6. Conclusions

A physical model of combined heat and mass transfer in a turbulent gas–vapor–drop ducted flow has been developed. In this model, the liquid phase represents a system of localized sinks of heat and localized sources of vapor mass and friction between the phases. To calculate gas phase turbulent characteristics, the Nagano–Tagawa LRN E–ε model was used, modified to the case of a flow with a contained dispersed phase. A closed system of transfer equations is composed, which includes the continuity equation, equation of flow in the longitudinal direction, energy equation with a source term, diffusion equation for the vapor–gas mixture, and the heat-and-mass transfer equation for a single drop. In the model, the precipitation of drops onto the wall and heat transfer due to immediate drop/wall contacts are taken into account.

A numerical heat and mass transfer study of a turbulent two-phase gas–vapor–drop ducted flow was performed. The data were obtained for a wide range of flow conditions and thermal parameters at the inlet to the duct.

With increasing mass concentration of liquid drops, a considerable intensification of heat- and mass transfer processes in the two-phase flow is observed, with a corresponding increase in the fraction of the heat spent on the phase transition and on the heat transfer due to immediate drop/wall.

It is shown that an increase in the initial drop diameter decreases the rate of heat transfer between the duct wall and the gas–vapor–drop mixture, whereas, in this case, the wall friction increases only slightly.

An increase in the mass concentration of air at the duct inlet considerably enhances the rate of heat

transfer, but, in this case, the region occupied by the two-phase flow becomes shorter. Both the gained data on the flow dynamics and heat transfer data were compared with available experimental results; a good agreement with previous findings was obtained.

Acknowledgements

This work was supported by the Russian Foundation for Basic Research (grant RFBR 01-02-16994 and 02-02-06327-mac) and by the Ministry of Education of the Russian Federation (grant TOO-1.2-260).

References

[1] M.A. Styrikovich, V.S. Polonsky, G.V. Tsiklaury, Heat and Mass Transfer and Hydrodynamics in Two-Phase Flows of Nuclear Power Station, Nauka, Moscow, 1982, in Russian.
[2] J.W. Hodgson, R.T. Saterbak, J.E. Sunderland, An experimental investigation of heat transfer from a spray cooled isothermal cylinder, ASME J. Heat Transfer 90 (4) (1968) 457–463.
[3] T. Aihara, M. Taga, T. Haraguchi, Heat transfer from a uniform heat flux wedge in air-water mist flow, Int. J. Heat Mass Transfer 22 (1) (1979) 51–60.
[4] K. Hishida, M. Maeda, S. Ikai, Heat transfer from a flat plate in two-component mist flow, ASME J. Heat Transfer 102 (3) (1980) 513–518.
[5] V.I. Terekhov, M.A. Pakhomov, Numerical study of heat transfer in a laminar mist flow over a isothermal flat plate, Int. J. Heat Mass Transfer 45 (10) (2002) 2077–2085.
[6] X. Li, J.L. Gaddis, T. Wang, Modeling heat transfer in a mist/steam impinging jet, ASME J. Heat Transfer 123 (6) (2001) 1086–1092.
[7] Y. Koizumi, T. Ueda, H. Tanaka, Post dryout heat transfer to R-113 upward flow in a vertical tube, Int. J. Heat Mass Transfer 22 (8) (1979) 669–678.
[8] A.G. Rane, S.-Ch. Yao, Convective heat transfer to turbulent droplet flow in circular tubes, ASME J. Heat Transfer 103 (4) (1981) 679–684.
[9] K. Mastanaiah, E.N. Ganic, Heat transfer in two-component dispersed flow, ASME J. Heat Transfer 103 (2) (1981) 300–306.
[10] A.I. Leont'ev, Propagation of limiting laws of friction and heat transfer on a turbulent stream regimes of a gas/liquid flows, Proc. Siberian Division of Academy Sciences of USSR. Ser. Technical Sciences 10 (7) (1984) 47–58.
[11] V.I. Terekhov, M.A. Pakhomov, A.V. Chichindaev, Heat and mass transfer in the developed turbulent two-component gas–vapor and droplet flow, J. Eng. Phys. Thermophys. 74 (2) (2001) 331–338.
[12] V.I. Terekhov, M.A. Pakhomov, A.V. Chichindaev, Effect of evaporation of liquid droplets on the distribution of parameters in a two-species laminar flow, J. Appl. Mech. Tech. Phys. 41 (6) (2000) 1020–1028.
[13] S. Sikalo, N. Delalic, E.N. Ganic, Hydrodynamics and heat transfer investigation of air-water dispersed flow, Int. J. Exp. Thermal Fluid Sci. 25 (7) (2002) 511–521.
[14] R.G. Deissler, Analysis of turbulent heat transfer, mass transfer, and friction in smooth tubes at high Prandtl and Schmidt numbers, NACA TR 1210, Washington DC, USA, 1955.
[15] Y. Nagano, M. Tagawa, An improved (k–ε) model for boundary layer flow, ASME J. Fluids Eng. 109 (1) (1990) 33–39.
[16] A.A. Shraiber, L.B. Gavin, V.A. Naumov, et al., Turbulent Flows in Gas Suspensions, Hemisphere, New York, 1990, p. 50.
[17] E.P. Volkov, V.A. Pershukov, L.I. Zaichik, Numerical Modeling of Combustion of Solid Fuel, Nauka, Moscow, 1994, in Russian.
[18] Z. Mansoori, M. Saffar-Avval, H. Basirat-Tabrizi, G. Ahmadi, Modeling of heat transfer in turbulent gas–solid flow, Int. J. Heat Mass Transfer 45 (6) (2002) 1173–1184.
[19] A. Berlemont, M.S. Grancher, G. Gousbet, Heat and mass transfer coupling between vaporizing droplets and turbulence using Lagrangian approach, Int. J. Heat Mass Transfer 38 (16) (1995) 3023–3034.
[20] C.T. Crowe, Review: Numerical models for dilute gas-particles flows, ASME J. Fluid Eng. 104 (3) (1982) 297–303.
[21] S.I. Isaev et al., in: A.I. Leont'ev (Ed.), Theory of Heat and Mass Transfer, Publishing House of Bauman Moscow State Technical University, Moscow, 1997, in Russian.
[22] M.C. Yuen, L.W. Chen, Heat transfer measurements of evaporating liquid droplets, Int. J. Heat Mass Transfer 21 (5) (1978) 537–542.
[23] I.N. Gusev, E.I. Guseva, L.I. Zaichik, Deposition of particle on channel walls in a turbulent flow, J. Eng. Phys. Thermophys. 59 (5) (1990) 735–742.
[24] H. Schlichting, Boundary Layer Theory, McGraw-Hill, New York, 1979.
[25] I.V. Derevich, Statistical modelling of mass transfer. Calculation results in turbulent dispersed flow-2, Int. J. Heat Mass Transfer 43 (19) (2000) 3725–3734.
[26] J.D. Anderson Jr. et al., in: J.F. Wendt (Ed.), Introduction to Computational Fluid Dynamics, Springer, Berlin, 1992, pp. 112–113, pp. 170–172.
[27] J.G.M. Eggels, F. Unger, M.H. Weiss, et al., Fully developed pipe flow: a comparison between direct numerical simulation and experiment, J. Fluid Mech. 268 (1994) 175–209.
[28] A.Yu. Varaksin, A.F. Polyakov, Experimental study of fluctuations of bidispersed particles velocity moving in turbulent flow of air, in: Proceedings of XII Seminar-School for Young Scientists and Specialists on the Problems of Gas Dynamics and Heat and Mass Transfer in Power Plants, Moscow, May 25–28 1999, pp. 207–210 (in Russian).
[29] T.J. Cramer, C.A. Depew, Experimentally determined mean flow characteristics of gas–solid suspension, ASME J. Fluids Eng. 94 (2) (1972).
[30] W.S.J. Uijetterwaal, R.V.A. Oliemans, Particle dispersion and deposition in direct numerical and large eddy simulations of vertical pipe flow, Phys. Fluids A 8 (10) (1996) 2590–2604.

[31] A.Yu. Varaksin, A.F. Polyakov, Experimental study of fluctuations of particles velocity in turbulent flow of air in a pipe, High Temperature 38 (5) (2000) 792–798.
[32] A.Yu. Varaksin, Yu.V. Polezhaev, A.F. Polyakov, Experimental investigation of the effect of solid particles on turbulent flow of air in a pipe, High Temperature 36 (5) (1998) 767–775.
[33] Y. Tsuji, Y. Morikawa, H. Shiomi, LDV measurements of an air-solid two-phase flow in a vertical pipe, J. Fluid Mech. 139 (1984) 417–434.